Journal of Non-Newtonian Fluid Mechanics 351 (2026) 105686

Contents lists available at ScienceDirect

Journal of Non-Newtonian Fluid Mechanics

journal homepage: www.elsevier.com/locate/jnnfm

Full length article

Formulation and scaling of refractive index-matched non-Newtonian blood analogues for optical flow studies

J.A. Lowe [a], E.P.F. Barton [a], R.L. Lewis [a], J.-B.R.G. Souppez [b], W.H. Ho [c], S.G. Yazdi [d], L.J. Leslie [a], P.T. Griffiths [a], P.H. Geoghegan [a,*]

[a] School of Engineering & Innovation, Aston University, Birmingham, B4 7ET, United Kingdom
[b] Department of Engineering, School of Architecture, Built Environment, Computing and Engineering, Birmingham City University, Birmingham, B4 7XG, United Kingdom
[c] Department of Mechanical Engineering, University of Cape Town, Rondebosch, Cape Town, 7700, South Africa
[d] Evasc Neurovascular, Vancouver, BC, Canada

ARTICLE INFO

Keywords:
Non-Newtonian blood analogue
Shear-thinning
Power-law rheology
Refractive-index matching
Dynamic similitude
Rheological characterization
Optical flow measurements
Particle image velocimetry
Haemodynamic modelling

ABSTRACT

Blood is a complex non-Newtonian fluid exhibiting shear-thinning and viscoelastic behaviour. Experimental modelling of arterial flows is essential for cardiovascular disease research, yet many *in-vitro* studies approximate blood as Newtonian due to practical constraints. Recent computational and limited experimental work has demonstrated this assumption can lead to significant differences in velocity and wall shear stress estimations. While non-Newtonian analogues have been used, studies often omit scaling methodology or rely on dimensionless numbers neglecting shear-dependent behaviour, reducing physiological relevance. This work addresses these limitations with an approach for formulating, characterizing, and scaling a refractive index (RI) matched non-Newtonian analogue for optical-based flow measurements, composed of water, glycerol, urea and xanthan gum (XG). Urea offers an inexpensive, safe alternative to salts like sodium iodide, enabling RI adjustment while maintaining physiologically relevant viscosities. The literature suggests small concentrations of XG can be added to induce shear-thinning and viscoelastic behaviour, though rheology is sensitive to batch variability, temperature, and pH. Rheological characterization revealed that achieving physiologically relevant shear-thinning behaviour required higher XG concentrations than anticipated, reinforcing the need for rheological characterization of each preparation. For the first time, a four-component analogue was formulated that matches both the RI needed for optical studies, and the power-law exponent of whole blood, enabling dynamic scaling that accounts for shear-dependent viscosity within a power-law representation of blood rheology. Results indicate that characterization of each analogue fluid is necessary, as previously reported ratios and properties cannot be assumed. Although demonstrated for arterial flows, the framework is applicable to a broader range of shear-thinning systems. This study provides a framework for future non-Newtonian optical-based haemodynamic investigations that improves representation of shear-dependent rheology through rheological characterization and dynamic similitude.

1. Introduction

Accurate experimental modelling of arterial flows is critical for advancing vascular disease research and pre-clinical testing of medical devices. Haemodynamics strongly influence atherosclerosis initiation, pathogenesis and outcomes of surgical intervention, making *in-vitro* studies essential for informing clinical practice and validating computational research [1]. Experimental modelling of arterial flows is also emphasized under ASME V&V 40 guidelines, which call for rigorous verification and validation of computational models using experimental data to ensure credibility in medical device evaluation [2]. Compliance with the ASME V&V 40 framework is increasingly expected by several regulatory bodies for submission, including the FDA (USA), EMA (EU), and MHRA (UK) [3].

Although constitutive rheological models can be employed relatively simply in computational fluid dynamics to capture blood's non-Newtonian behaviour, experimental studies often simplify blood as a Newtonian fluid due to practical constraints. This approach is typically justified by the mean shear rates ($\dot{\gamma} \geq 100\,s^{-1}$) present in large arteries

* Corresponding author.
E-mail address: p.geoghegan@aston.ac.uk (P.H. Geoghegan).

https://doi.org/10.1016/j.jnnfm.2026.105686
Received 8 May 2026; Received in revised form 28 October 2026; Accepted 29 October 2026
Available online 9 November 2026
0377-0257/© 2026 The Authors. Published by Elsevier B.V. This is an open access article under the CC BY license (http://creativecommons.org/licenses/by/4.0/).

($D \geq 5\,\text{mm}$) such as the aorta or carotid vessels, with local wall shear gradients higher, leading many to assume that non-Newtonian effects are minimal [4–8]. However, both computational and the limited experimental evidence available suggest that this assumption can introduce inconsistencies in velocity distribution and wall shear stress (WSS) estimation, which is a key metric in assessing endothelial dysfunction and cardiovascular diseases. These differences become increasingly important in situations where the shear rates are significantly lower than $\dot{\gamma} < 100\ \text{s}^{-1}$ [9–12].

Whole blood is a suspension of cellular material in plasma, exhibiting several non-Newtonian behaviours, predominantly shear-thinning, arising from the deformability and aggregation of red blood cells (RBCs) [13–20]. At low shear rates ($\dot{\gamma} \leq 100\,\text{s}^{-1}$), the apparent viscosity increases exponentially due to the formation of rouleaux [13,20]. Conversely, as the shear rate increases ($\dot{\gamma} > 100\,\text{s}^{-1}$), apparent viscosity decreases as these structures break down and the RBCs begin to elongate and align with the flow. At high shear rates ($\dot{\gamma} \geq 1000\,\text{s}^{-1}$), the viscosity of blood at 37 °C typically plateaus between $3.5\,\text{mPa s} \leq \mu_\infty \leq 5.5\,\text{mPa s}$ [7,21].

Blood also exhibits weak viscoelasticity due to the continual deformation of RBCs and the reversible formation and breakdown of rouleaux structures leading to the periodic storage and release of elastic energy [16]. While the elastic behaviour is considered weak, its contribution is more pronounced at higher oscillation frequencies such as during increased heart rates. In haemodynamic studies of larger arteries ($D \geq 5\,\text{mm}$), viscoelastic effects are generally considered negligible compared to the dominant shear-thinning behaviour [22]. Moreover, blood has been shown to exhibit minimal thixotropic behaviour (relaxation time 0 s–3 s), due to the time required for the rouleaux structure to reach equilibrium. It also exhibits yield stresses ($\sigma_y = 1\,\text{mPa}–5\,\text{mPa}$) arising from the stress required to disrupt the RBC aggregates and allow flow. Given the near-negligible thixotropic and viscoplastic effects at physiologically relevant shear rates, these behaviours were not quantified in the present work. Blood rheology is influenced by numerous factors such as haematocrit, sample handling and measurement protocol, pathologies like sickle cell anemia and diabetes, and high cholesterol [17,21,23,24]. Although density is also affected by some of these factors, it is typically measured as $\rho = 1060\,\text{kg m}^{-3}$ [7].

Advances in computational modelling have enabled researchers to employ constitutive rheological models to capture blood's non-Newtonian behaviour in simulations of arterial flows [20,25,26]. Numerous *in-silico* studies have reported markedly different haemodynamic effects when Newtonian behaviour is assumed, including deviations in velocity fields, pressure distributions, WSS and oscillatory shear metrics [10,11,23,27–30]. However, limited computational studies have also questioned the significance of these differences, suggesting that Newtonian approximations could remain acceptable when exploring certain metrics, geometries or flow conditions [31–33].

Key experimental studies employing non-Newtonian analogue fluids are summarized in Table 1. These works have compared flow behaviour against Newtonian analogues, reporting that differences in velocity distribution, recirculation size and length, WSS estimations, and transition to turbulence [8–10,34–37]. However, the reported magnitude and direction of these differences remain inconsistent. For example, there is disagreement over whether a Newtonian assumption over- or underestimates WSS or state both can happen depending on the geometric location [9,35,38–40]. These differences may arise from limitations frequently applied in experiments, such as rigid-wall modelling, steady inflow conditions, and simplified geometries.

Experimental research also faces several additional challenges meaning Newtonian assumptions remain common. Optical flow visualization techniques like particle image velocimetry (PIV) require transparent analogue fluids with a refractive index (RI) matching that of the flow phantom as mismatches can introduce significant image distortion and increase measurement uncertainty [7,48]. Non-optical techniques like ultrasound and MRI do not require transparency or RI-matching, though properties such as acoustic impedance and magnetic susceptibility become critical. Phantom material selection introduces constraints on analogue fluid design due to optical compatibility. Polydimethylsiloxane (PDMS) silicones, particularly SYLGARD 184, with a RI $1.40 < \theta < 1.43$, is widely used for the manufacture of both rigid and compliant arterial phantoms [7,49]. Recent advances in 3D printing have enabled flow phantoms to be manufactured from stereolithography (SLA) resins, though these are predominantly limited to rigid models and are scarcely used due to the typically high RI ($\theta = 1.51$) in comparison to PDMS, although additional coatings are being explored to improve optical properties [50–52]. 3D printing of soft materials can replicate more physiologically realistic compliance, though their application is similarly limited by their optical properties [53].

To achieve RI-matching, the fluid's density and rheological properties will likely differ slightly from that of blood and hence require an appropriate scaling methodology to achieve similitude. Additionally, it is common to scale up geometries *in-vitro* to improve spatial resolution of measurements and enable compatibility with flow circuits. For Newtonian fluids, similitude can be achieved by scaling flow conditions to match the Reynolds (Re) and Womersley (α) numbers between systems, respectively:

$$Re = \frac{\rho \bar{u} D}{\mu}, \qquad \alpha = \frac{D}{2}\sqrt{\frac{\omega \rho}{\mu}}, \tag{1}$$

where ρ is fluid density, $\bar{u}$ is the average fluid velocity at the inlet, D is vessel inner diameter, μ is the dynamic viscosity and ω is the angular frequency ($\omega = 2\pi f$). For Newtonian scaling, the high-shear viscosity (μ_∞) of blood is often used as an approximation for μ. However, these definitions assume viscosity is constant and therefore do not capture the shear-thinning properties accurately, hence using them could introduce errors in measurements [9].

Crucially, as evidenced in Table 1, almost all experimental studies employing non-Newtonian analogue fluids scale flow boundary conditions using the Newtonian definitions with the high-shear viscosity of whole blood and the analogue fluid. Some also omit their scaling methodology completely [28]. As viscosity varies with shear rate, this approach does not ensure dynamic similarity between the analogue fluid and physiological blood flow, especially in regions of low shear ($\dot{\gamma} \leq 100\,\text{s}^{-1}$). Therefore, while analogue fluid studies have demonstrated that non-Newtonian behaviour can influence haemodynamics, the absence of an appropriate scaling framework that incorporates shear-dependent behaviour limits the physiological relevance of their conclusions.

Consequently, this work addresses these limitations by presenting a methodology for the formulation of an RI-matched non-Newtonian blood analogue, inclusive of rheological characterization and scaling approach that considers shear-dependent behaviour. For the first time, a four-component analogue was developed with a power-law index matching whole blood, enabling similitude, within the proposed power-law scaling framework, for optical flow visualization techniques. The procedure to achieve dynamic similarity is presented together with an experimental comparison between a Newtonian fluid and the appropriately scaled non-Newtonian fluid. This comparison is intended to demonstrate the influence of rheology and scaling strategy on the measured flow field. It does not constitute direct validation of the scaled non-Newtonian flow against physiological blood flow. This work also highlights the importance of batch-specific rheological evaluation rather than adopting formulations from literature without verification, as both environmental factors and constituent variability can alter fluid behaviour.

The remainder of this paper is structured as follows. Section 2 presents the power-law model as a method to characterize non-Newtonian fluids like blood. Section 3 introduces the current blood analogues used in experimental measurements and their associated limitations. Section 4 provides a dynamic scaling approach incorporating

Table 1
Summary of key experimental studies using non-Newtonian blood analogues.

Author	Arterial model and phantom material	Constituents	Rheological law (and constant coefficients)	Density ($kg\,m^{-3}$)	RI	Scaling method	Analysis method
Yi et al. [28]	Cerebral Aneurysm; Watershed XC 11122 materials	W, XG	Power-law @ 24 °C $n = 0.572$; $K = 32.3\,mPa\,s^n$	930–940	–	–	PIV
Jasikova et al. [41]	CAB with aneurysm; SYLGARD 184	W, G, D	$\mu_\infty = 4.4\,mPa\,s$ @ 37 °C	1020	–	Re; α	PIV
DiCarlo et al. [42]	CAB with stenosis; PDMS	W, G, NaI, XG	Cross model for $\dot{\gamma} > 1\,s^{-1}$	–	–	Re	SPIV
Biswas et al. [34]	Straight tube; butyrate	Porcine blood with 10% sodium citrate	$2.76 \leq \mu_\infty \leq 3.42\,mPa\,s$ at $\dot{\gamma} = 1000\,s^{-1}$ @ 37 ± 0.3 °C	1030	–	Re	DUS
Huh et al. [43]	Straight stenosis; SYLGARD 184	W, G, NaI, XG	Casson model; $2.91 \pm 0.005 \leq \mu_\infty \leq 3.5 \pm 0.005\,mPa\,s$ at $\dot{\gamma} = 10^5\,s^{-1}$	1304 ± 7.7–1309 ± 6.44	1.413	Re	PIV
Completo et al. [44]	Slit cell	W, G, XG	Power-Law; Casson; Herschel Bulkley (values omitted)	–	1.33791–1.4029	Re	μPIV
Deplano et al. [45]	AAA; silicon	W, G, Sodium salt, XG	$\mu_\infty = 4.039\,mPa\,s$ @ 25 ± 0.01 °C	1099	–	Re; α	PIV
Walker et al. [46]	Straight tube; acrylic	W, G, XG	–	–	–	Re	PIV
Anastasiou et al. [35]	Small bifurcating artery; polymeric chip	W, G, XG	Herschel-Bulkley model; $3.32 \leq \mu_\infty \leq 5.03\,mPa\,s$	1052–1083	–	Re	μPIV
Gray et al. [9]	Distal anastomosis; u-PVC with borosilicate glass	W, G, XG, (two mixtures)	Power-law; $n = 0.63$ and $K = 35.1\,mPa\,s^n$; $60.6\,mPa\,s^n$	1002–1089	–	Re_{PL}; St; n	PIV
Gijsen et al. [47]	CAB; PMMA	W, NaSCN, XG	Carreau-Yasuda; Viscoelastic characterization	–	–	Re	LDA

CAB - Carotid Artery Bifurcation, AAA - Abdominal Aortic Aneurysm, W - Water; G - Glycerol; XG - Xanthan Gum; D - Dextran; NaI - Sodium Iodide; NaSCN - Sodium thiocyanate, PIV - Particle Image Velocimetry; SPIV - Stereoscopic PIV; μPIV - Micro-PIV; LDA - Laser Doppler Anemometry.

the power-law model for non-Newtonian fluids. Section 5 outlines the development and characterization of a scalable, RI-matched, shear-thinning analogue suitable for optical flow visualization. Section 5.3 presents a practical example and experimental flow comparison using the developed analogue. Finally, Section 6 summarizes the main findings and provides recommendations for future experiments using non-Newtonian blood analogues.

2. Non-Newtonian modelling of blood

While studies have previously used a Newtonian approximation for blood, justified by the moderate mean arterial shear rates present in large vessels, assuming Newtonian behaviour can still cause errors in local haemodynamic estimations. This is especially true in regions of complex anatomy, where regions of low shear, recirculation and secondary flows prevail. The differences in observations of both computational and experimental studies comparing Newtonian and non-Newtonian modelling originate from variations in viscosity across the flow domain.

When blood's non-Newtonian behaviour is considered, the behaviour can be modelled using numerous constitutive equations. The power-law model is the simplest model and predicts the apparent viscosity ($\mu(\dot{\gamma})$) or shear stress (τ) at a given shear rate using two parameters, it is defined as follows:

$$\mu(\dot{\gamma}) = K\dot{\gamma}^{n-1}, \qquad \tau = K\dot{\gamma}^{n}, \tag{2}$$

where K is the power-law consistency index and n is the power law exponent. For a shear-thinning fluid, $n < 1$, for a shear thickening fluid $n > 1$, and for a Newtonian fluid $n = 1$.

Alternative rheological models exist, such as the three parameter Sisko model, which incorporates an infinite-shear viscosity (μ_∞) alongside the power-law terms, or more complex models such as the Carreau-Yasuda (5 parameter) or Casson model (4 parameter). These can capture the low- and high-shear asymptotes more accurately, however the power-law model was deliberately chosen based on critical fluid formulation and optical constraints. Specifically, while the Sisko model accounts for the high-shear Newtonian plateau, using it to scale flow between systems would require all three terms (n, K, μ_∞) to be precisely prescribed in order to satisfy similitude and the additional dimensionless group created as a result of the extra term [9]. Furthermore, introducing additional parameters increase the sensitivity of the analogue to environmental factors such as temperature, significantly complicating dynamic scaling between systems. As a result, the two-parameter power-law model provides an optimal, feasible balance that preserves the dominant shear-thinning physics within the shear rates regimes typical or large arterial vessels ($D \geq 5\,mm$).

Blood's power-law constants are sensitive to the shear fitting range, measurement protocol, and underlying pathologies. For whole blood n has been reported between $0.5 < n < 0.983$ with a K value between $0.9\,mPa\,s^n < K < 17.5\,mPa\,s^n$ [9,54–59]. Eliminating the studies reporting with non-physiological temperatures, disease or unclear fitting procedure, these ranges can be reduced to between $0.630 < n < 0.716$ and $12.3\,mPa\,s^n < K < 16.7\,mPa\,s^n$.

In this work, blood was assumed to have a power-law exponent of $n = 0.677$ and consistency index of $K = 16.2\,mPa\,s^n$. Meanwhile the high-shear viscosity for Newtonian comparisons was assumed to be $\mu_\infty = 3.5\,mPa\,s$, typical of many studies assuming Newtonian behaviour. While this approximation has been used for many studies, there are significant differences in theoretical flow behaviour. For instance, Fig. 1 compares cross-sectional behaviour of fully developed, laminar pipe flow of a Newtonian or non-Newtonian fluid at an identical flow rate typical of mean flow in the carotid artery. For a given flow rate (Q), the Newtonian ($u_N(r)$) and power-law ($u_{PL}(r)$) velocity profiles are defined as:

$$u_N(r) = \frac{2Q}{\pi R^2}\left(1 - \left(\frac{r}{R}\right)^2\right), \tag{3}$$

$$u_{PL}(r) = \frac{Q}{\pi R^2}\left(\frac{3n+1}{n+1}\right)\left(1 - \left(\frac{r}{R}\right)^{\frac{n+1}{n}}\right), \tag{4}$$

where $u(r)$ is velocity at a point, r, and R is the total radius. The differences shown in Fig. 1 highlight that even for basic flow conditions like flow in a straight pipe, Newtonian approximations for

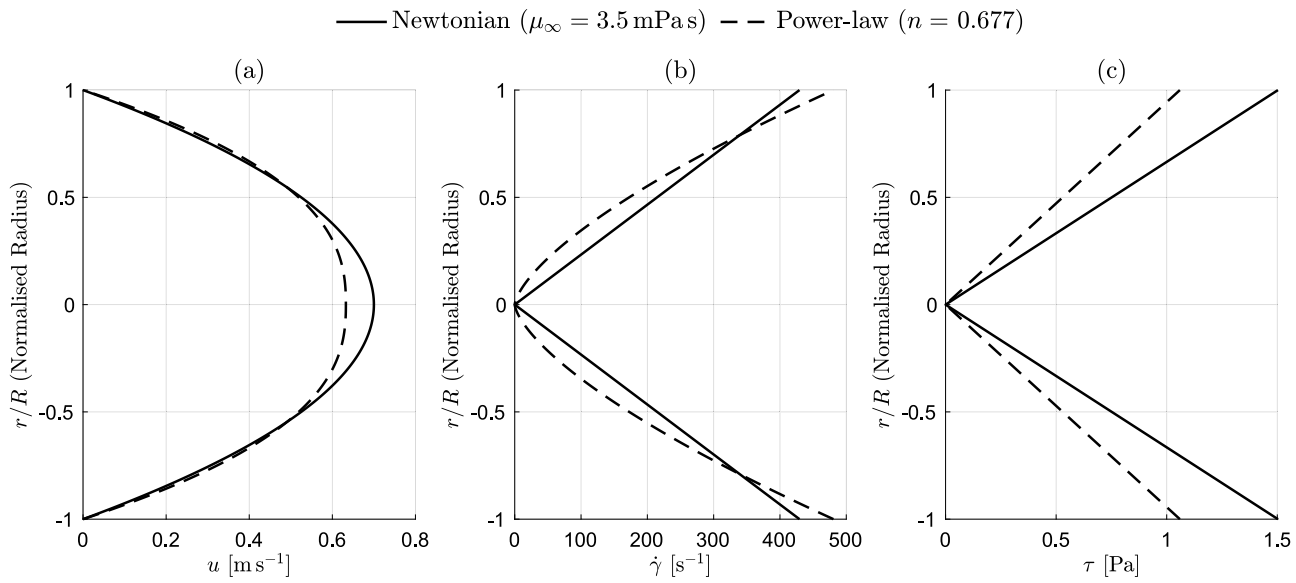


Fig. 1. Comparison of fully developed, laminar blood flow in a straight tube at a constant flow rate when blood is modelled as Newtonian using $\mu_\infty = 3.5$ mPa s and as a power-law fluid with $n = 0.677$, and $K = 16.2$ mPa s^n. (a) Velocity profile – non-Newtonian flow exhibits a reduction in the peak velocity and steeper near wall gradient compared to the Newtonian. (b) Shear profile (c) Viscosity profile.

blood could mislead interpretations. The power-law fluid produces a markedly blunted velocity distribution, elevated near-wall shear rates, a non-uniform viscosity field and significant differences in shear stress gradient. One physical limitation of the power-law model is that as $\dot{\gamma} \to 0$, $\mu(\dot{\gamma}) \to \infty$. In practice the viscosity would plateau hence error in the velocity profile towards the vessel centre is anticipated. While the velocity profile shows greater differences towards the centre of the pipe where the shear rate is lowest, the spatially varying viscosity and parabolic shear rate profile in the power-law fluid lead to large differences in shear stress near the wall. Consequently, WSS, a key marker for endothelial dysfunction would be distorted in any study employing a Newtonian approximation. These differences arise solely from how blood is modelled and should not be overlooked in haemodynamic measurements. Consequently, employing a Newtonian model results in an inadequate comparison for haemodynamics, reinforcing the need to incorporate non-Newtonian behaviour in both computational and experimental studies.

3. Review of blood analogues

3.1. Base Newtonian analogues

Non-Newtonian blood analogues typically start with a Newtonian base fluid, with additional components added to introduce non-Newtonian behaviours. Aqueous glycerol solutions are widely used for optical measurements of internal flows as they are generally inexpensive, safe and straightforward to make and can be easily RI-matched to PDMS phantoms [7,49]. A 61 : 39 glycerol:water mixture (by weight) closely matches SYLGARD 184's RI, and can be tuned by altering the component concentrations. However, the viscosity and density at room temperature ($\mu \approx 10.6$ mPa s, $\rho \approx 1160$ kg m^{-3}) exceed blood.

Matching Reynolds and Womersley numbers aids similitude, but exact replication of *in-vivo* conditions can be challenging, as fluid–structure interactions introduced with compliant phantoms can complicate pressure-flow behaviour. For non-optical studies, RI-matching is unnecessary and these challenges can be mitigated by sacrificing RI and using an aqueous solution of 10% glycerol with small amount of dextran to generate a fluid with viscosity in range of bloods ($\mu = 4.1$ mPa s) high-shear plateau [60].

RI tuning of Newtonian formulations with similar viscosity to blood can be achieved by adding salts (NaI, NaSCN, KSCN), though these introduce challenges including corrosiveness, toxicity and low chemical stability [49,61]. Safer, inexpensive alternatives include urea or xylitol [49]. Both additives have been shown to produce analogues with a suitable RI for SYLGARD 184, while also matching a range of high-shear viscosities reported for blood using different ratios. Solutions with urea provided RI tuning with minimal influence on the density and viscosity in contrast with NaI solutions, resulting in several recent studies implementing urea-based analogues [62,63].

Table 2 summarizes the main Newtonian formulations developed in literature. These formulations can achieve improved density and high-shear viscosity matching; however, their constant viscosity does not replicate blood's complex shear-dependent rheology. Consequently, dynamic similarity in haemodynamic experiments must rely on high-shear approximations unless non-Newtonian behaviours are modelled.

3.2. Non-Newtonian analogues

The addition of low concentrations of certain polymers to a Newtonian base fluid can introduce shear-dependent behaviour. Although biologically derived fluids have been explored, they offer limited advantages over polymer-based alternatives. For example, one study used a modified platelet rich plasma fluid to mimic blood rheology and thrombus formation in PIV measurements [68]. Although the fluid reproduced the shear-thinning behaviour of porcine blood, this comparison is limited because porcine blood differs from human blood in both rheology and RBC aggregation, typically exhibiting higher viscosity than human blood at a given shear rate [69]. Furthermore, thrombus formation was artificially induced and occurred at unrealistically short timescales. Schürmann et al. [70] developed an analogue fluid of ghost porcine RBCs, creating a cellular fluid with suitable rheological properties and scattering properties for PIV measurements, though RI was not reported. Generally, biologically derived fluids are severely limited by high fluid cost, ethical concerns, short shelf life, and safety considerations, meaning they are only used for specific applications such as studying hemolysis.

Polymer-based non-Newtonian analogues have therefore become standard. Table 3 summarizes the key non-Newtonian developmental studies for optical flow measurements. Xanthan gum (XG) is a natural polysaccharide that has been used to induce shear-thinning behaviour in blood analogues [49,71,72]. It is soluble in both cold and hot

Table 2
Summary of Newtonian blood analogues for optical flow visualization reported in fluid development studies.

Author	Constituents	Density $(\mathrm{kg\,m^{-3}})$	Viscosity (mPa s)	RI	Notes
Yazdi et al. [7]	Blood; SYLGARD 184	1060 @37 °C	2.9–4.37 @37 °C	1.413	
Yazdi et al. [7]	W-G (60:40)	1160	10.6 @21 °C	1.417	
Brindise et al. [49] and Najjari et al. [61]	W-G-NaI	1211–1229; 1456 ± 10	3.117–4.616; 5.45 ± 1.27	1.4131–1.4143; 1.495	Multiple safety concerns; tunable to different viscosities and RI
Shuib et al. [64]	W-G-NaCl	1080	6.23	–	
Nguyen et al. [65]	EtOH-DEP	–	$\nu = 0.003\,454\,\mathrm{m\,s^{-2}}$ @48.5 °C	1.486	Multiple safety concerns
Najjari et al. [61]	W-G-NaSCN	–	–	1.417–1.495	Multiple safety concerns
Najjari et al. [61]	W-KSCN	1429 ± 10	$\nu = 2.02 \times 10^{-6}\,\mathrm{m\,s^{-2}}$ @25 °C	1.484	Multiple safety concerns
Brindise et al. [49]	W-G-U	1114–1141	3.534–5.178	1.4118–1.4132	Tunable to different viscosities and RI
Brindise et al. [49]	W-G-Xy	1152–1154	2.957–4.033	1.4118–1.420	Tunable to different viscosities and RI
Doutel et al. [66] and Carvalho et al. [67]	W-DMSO	1057; 1072	3.5; 3.153		

W - Water; G - Glycerol, NaI - Sodium Iodide; NaCl - Sodium Chloride; EtOH - Ethanol; DEP - Diethyl phtalate; NaSCN - Sodium Thiocyanate; KSCN - Potassium Thiocyanate; U - Urea; Xy - Xylitol; DMSO - Dimethyl-sulfoxide.

Table 3
Summary of non-Newtonian blood analogue development studies for optical flow visualization.

Author	Constituents	Rheological Characteristics	Density $(\mathrm{kg\,m^{-3}})$	RI	Notes
Brindise et al. [49]	W, G, U, XG W, G, NaI, XG (various concentrations)	Solutions with 0.02% by wt XG mimicked viscoelasticity best	1114–1229	1.4118–1.4143	–
Clauser et al. [68]	Plasma-based fluid with high platelet concentration and low erythrocyte concentration.	Shear-thinning observed; $\mu_\infty = 3.67 \pm 0.07$ mPa s at 1000 $\mathrm{s^{-1}}$	–	1.347–1.384	Biological fluid; artificial thrombus formation
Najjari et al. [61]	W, G and XG W, G, NaI and XG (in various concentrations); W, G, NaSCN and XG (in various concentrations)	Salt concentration influenced rheology; Reduced shear-thinning with temperature	1050–1678	1.373–1.495	–
Campo-Deaño et al. [16]	DMSO, HA & PAA; DMSO & XG; Sucrose, HA, & PAA; Sucrose & XG	All analogues similar to human blood with anticoagulant	–	1.39–1.41	–
Brookshier and Tarbell [72]	W, G, XG (in various concentrations)	Similar viscoelasticity for a range of haematocrit	–	–	–
Mann and Tarbell [71]	W, G as base; XG (0.0375% wt); PAA (0.02% wt)	XG superior viscoelasticity; both similar shear-thinning	–	–	Fails to simulate elastic properties accurately; XG better

W - Water; G - Glycerol; U - Urea; XG - Xanthan gum; NaI - Sodium Iodide; NaSCN - Sodium thiocyanate; DMSO - Dimethyl-sulfoxide; HA - Hyaluronic acid; PAA - Polyacrylamide.

water, but requires extensive mixing to fully hydrate and dissolve into the solution. In addition to shear-thinning properties, the addition of between 0.0075% and 0.075% by weight XG to aqueous glycerine solutions with between 40% to 50% glycerol replicated the viscoelastic behaviour of porcine blood across a range of haematocrits [72]. Subsequent studies have demonstrated that XG can also be added to RI-matched three-component Newtonian solutions such as water-glycerol-urea or water-glycerol-NaI to achieve suitable viscoelastic properties while maintaining optical accessibility [16,49,61].

Polyacrylamide (PAA) is another water-soluble polymer that has been used to mimic the non-Newtonian properties of blood. However, in a comparative study focused on the rheology of PAA and XG solutions comprised of water and sodium chloride (NaCl), PAA was found to be inferior due to its elasticity, leading to a peak wall shear rate 2–3 times higher than bovine blood [71]. Although optical properties were not investigated, a subsequent, RI matched study using dimethyl-sulfoxide (DMSO), and either hyaluronic acid (HA) or sucrose reported similar findings [16]. Like porcine blood, bovine blood exhibits different rheological properties to human blood, with near constant viscosity behaviour and therefore limiting the clinical relevance of this work [73].

Two studies have proposed the addition of nylon particles (7–8 μm) to aqueous glycerine solutions for acoustic-based flow measurements [74,75]. The dimensions and density of the particles are similar to RBCs and also undergo aggregation at low-shear, mimicking shear-thinning behaviours. Rheological measurements showed the fluid could mimic blood at a range of haematocrits by further adding detergent, although the size of the nylon particles make them unsuitable for optical based measurements which rely on seeded, neutrally buoyant particles of similar dimension.

Overall, while several polymers and biological analogues have been trialled to reproduce the rheological properties of human blood, XG remains the most commonly used polymer due to its ability to induce shear-thinning behaviour whilst exhibiting low elasticity, and commercial availability. Nonetheless, it is important to note that many formulations have been compared against animal blood, which can have substantially different rheological properties to human blood, thereby limiting physiological relevance. Additionally, XG-based formulations have several challenges that prevent direct implementation of ratios reported in developmental studies without rheological characterization.

3.3. Challenges with xanthan gum analogues

In both developmental and experimental haemodynamic studies employing XG-base non-Newtonian analogues, the variability of XG-based solutions has been largely overlooked. This is despite evidence

that rheological properties can differ substantially between batches of XG from different manufacturers, and even from the same source [76]. For example, large differences in both the storage modulus (G') and loss modulus (G'') were observed in 1% aqueous XG solutions, along with variation in power-law fits to steady-shear data, suggesting alterations in shear-thinning behaviour and indicating that the analogue fluid properties cannot be assumed. G' and G'' represent elastic and viscous contributions to the fluid. These findings highlight the need for batch-specific rheological characterization.

Temperature and salt concentration jointly influence the rheology of XG solutions. Viscosity generally decreases and shear-thinning behaviour diminishes with increasing temperature, but for dilute XG solutions, the XG molecules can undergo a sudden structural transition, causing viscosity to rise. This typically occurs around 33 °C to 38 °C for water-XG mixtures, however the presence of salts for RI tuning can lower the transition temperature [77,78]. The presence of salts additionally reduce both the shear-thinning and viscoelastic properties for a given XG concentration [61]. A 10 °C difference in temperature in solutions of water-glycerol-XG with NaI or NaSCN was found to alter the apparent viscosity by approximately 20%, though elasticity was much less sensitive. In solutions containing urea to tune RI, the influence of concentration on viscoelastic properties was negligible in contrast to NaI [49].

A low pH (<5) significantly reduces shear-thinning behaviour of XG solutions [79,80]. At low concentrations (<0.2%) such as those typically used in blood analogues, this effect is increasingly significant. Moreover, for analogues containing urea, hydrolysis can occur, producing small amounts of ammonia and CO_2, increasing pH and hence affecting fluid rheology and RI. Because of this, routine monitoring is essential to ensure analogue stability.

4. Dynamic scaling of non-Newtonian blood analogues

When blood is assumed Newtonian, dynamic and kinematic similarity between *in-vivo* and experimental conditions can be achieved using Re and α numbers. This is however not the case for shear-thinning fluids as dynamic similarity can only be achieved if the shear-dependent behaviour is considered in a dimensional analysis when scaling flow conditions [9]. Using the high-shear viscosity to scale flow can lead to significant differences in flowrate boundary conditions and subsequent velocity fields and WSS estimations, affecting clinical relevance. Despite this, many experimental studies (introduced in Table 1) investigating haemodynamics with non-Newtonian analogues either do not report their scaling strategy or rely on Newtonian equations.

To accommodate shear-thinning behaviour, a dimensional analysis incorporating a constitutive rheological model like the power-law model is necessary. For a power-law fluid under pulsatile conditions, WSS can be expressed as a function of:

$$\tau_w = f\left(\bar{u}, D, \rho, K, n, \omega, \hat{u}\right), \tag{5}$$

where $\hat{u}$ is the peak-to-peak velocity. Applying the Buckingham-Pi theory, we derive 5 dimensionless groups:

$$\frac{\tau_w}{\frac{1}{2}\rho\bar{u}^2} = f\left[\frac{\rho D^n \bar{u}^{2-n}}{K}, n, \frac{\omega D}{\bar{u}}, \frac{\hat{u}}{\bar{u}}\right], \tag{6}$$

where $\frac{\tau_w}{\frac{1}{2}\rho\bar{u}^2}$ is the wall-stress coefficient, $\frac{\rho D^n \bar{u}^{2-n}}{K}$ is the generalized Reynolds number (Re_{PL}), $\frac{\omega D}{\bar{u}}$ is the Strouhal number (St) and $\frac{\hat{u}}{\bar{u}}$ is the pulsatility index. The power-law exponent is already non-dimensional and forms its own group. The Strouhal number replaces the Womersley number in scaling the pulsation frequency, although α can be obtained by combining Re and St as $\alpha = \frac{1}{2}\sqrt{Re \cdot St}$ [9]. For a Newtonian fluid, $n = 1$ and the generalized Reynolds number reduces to the classical Newtonian formulation if $K = \mu_\infty$. Matching all of these groups across fluid systems ensures dynamic similarity while accounting for shear-thinning.

Matching the non-dimensional power-law exponent (n) between systems is critical as it describes the degree of shear thinning and governs the velocity profile and shear distribution across the flow domain. Conversely, the consistency index (K) is a dimensional parameter that scales with the magnitude of the overall fluid viscosity. Consequently, the consistency index can differ between *in-vivo* and *in-vitro* as dynamic similarity is preserved by incorporating the consistency index into the generalized Reynolds number.

Furthermore, in large arterial vessels ($D \geq 5$ mm), shear-thinning dominates the flow behaviour, whereas viscoelastic effects remain weak at normal cardiac pulsation frequencies. Under these conditions, dimensionless parameters characterizing viscoelasticity, such as Weissenberg (Wi) and Deborah (De) numbers, are typically small ($Wi \approx 0.01$ and $De \approx 0.1$) for large vessels ($D \geq 5$ mm) [17]. Because viscous forces are dominant over elasticity, these parameters can be neglected. Consequently, while exact viscoelastic similitude could be pursued, it would significantly complicate both fluid formulation and RI tuning without altering the dominant shear-thinning flow physics. Despite this, in microvasculature, elasticity becomes more dominant and these numbers should be considered.

It should be noted that this framework focuses on replicating and scaling the shear-thinning behaviour of blood through the power-law model. Other non-Newtonian characteristics, including viscoelasticity, could potentially be incorporated through alternative scaling procedures based on additional rheological parameters and dimensionless groups. However, the objective of this study was to establish a practical framework for preserving the dominant shear-thinning behaviour. Inclusion of these effects would substantially increase the complexity of both the fluid formulation and scaling methodology, and was therefore considered beyond the scope of the present work.

5. Development and characterization of a power-law blood analogue fluid

This section presents the formulation and characterization of a shear-thinning blood analogue comprised of water, glycerol, urea, and XG. The analogue was designed to match the RI of a compliant SYLGARD 184 phantom, while also having the same power-law index for whole blood, enabling similitude using the dimensionless groups defined in Eq. (6).

5.1. Newtonian base fluid

A Newtonian base fluid was prepared using tap water, vegetable-derived glycerol (99.5%, Vegetableglycerine.co.uk), and urea prills (97.5%, Atom Scientific, UK) mixed in the ratio 45.64% water, 28.77% glycerol, and 25.58% urea by weight, following the low-viscosity solution described by Brindise et al. [49]. Water and urea were mixed for several hours to dissolve the prills before adding the glycerol. RI was then tuned by imaging a checkerboard grid through the phantom submerged in the same fluid. Glycerol or water were then added to increase or decrease the RI, respectively, following standard procedures for PIV [7]. Fig. 2 illustrates the phantom before and after RI matching.

The final ratio of the RI matched fluid was 45.21% water, 29.50% glycerol, and 25.29% urea by weight. RI was measured using a refractometer with wavelength $\lambda = 582$ nm (Mettler Toledo Easy R40) over a range of temperatures. The RI of the solution at 22 °C was $\theta = 1.4124 \pm 0.0001$. Triplicate rheology measurements were performed using steady-shear measurements with a 25 mm diameter, 1° cone-and-plate geometry and a gap of 73 μm on a Kinexus Prime rotational rheometer (NETZSCH Analysing and Testing, Selb, Germany) across a range of shear rates (5–500 s^{-1}). The base Newtonian viscosity was comparable to the reported high-shear viscosity of blood at all measured temperatures ($\mu = 4.06 \pm 0.049$ mPa s at 22 °C) but exceeded the reported viscosity value by Brindise et al. [49] for the base ratio, likely due to the slightly higher glycerol concentration, needed to achieve RI-matching

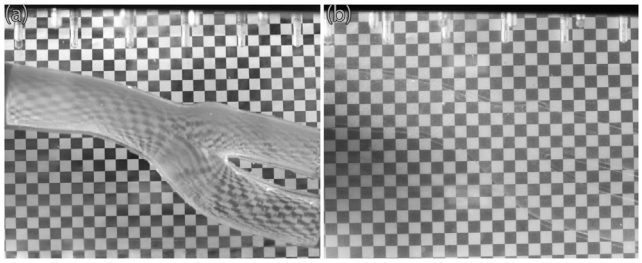


Fig. 2. (a) Filled compliant carotid artery bifurcation phantom imaged in air before RI matching, showing strong optical distortion. (b) The same phantom both filled with and submerged in the RI-matched fluid, resulting in reduced refraction and improved optical clarity necessary for flow visualization.

at a lower measurement temperature in the present analogue. Both RI and viscosity were observed to decrease linearly with increasing temperature with a RI of $\theta = 1.4119 \pm 0.0001$ and viscosity of $\mu = 3.93 \pm 0.047$ mPa s at 25 °C.

5.2. Non-Newtonian analogue

5.2.1. Steady-shear

XG (Healan Ingredients Ltd, UK) was incrementally added to RI-matched base solutions to induce shear-thinning behaviour. Concentration was optimized through rheological characterization until the power-law index at 22 °C matched the physiological power-law value ($n = 0.677$). The solution was agitated for 24 h after each addition to ensure full hydration and homogenous mixing, with RI checked daily to ensure minimal change from evaporation. A concentric cylinder (couette) was used to characterize flow across a broader range of shear rates (0.1−1000 s^{-1}) to fully capture the shear-dependent behaviour. Fig. 3 shows the steady-shear results across the five temperatures. Taylor–Couette instabilities were observed at shear rates $\dot{\gamma} \geq 500$ s^{-1} and were therefore omitted from further analysis. The onset of Taylor vortices when the inner cylinder exceeds a certain rotational speed leads to an uncharacteristic rise in apparent viscosity that does not reflect the properties of the fluid accurately. Across the studied temperatures, the overall viscosity and the degree of shear-thinning decreased with increasing temperature, reflected by a decrease in the consistency index and increase in the power-law index. At high shear rates, all temperatures tend to converge towards a similar apparent viscosity between 8.5 mPa s $< \mu_\infty <$ 9.5 mPa s, due to increased alignment of the XG molecules.

Power law constants were derived from the steady-shear data by a linear regression analysis of $\log(\mu(\dot{\gamma}))$, and $\log(\dot{\gamma})$ between the chosen shear limits. The gradient gives n and the intercept at $\log(\dot{\gamma})$ corresponds to $\log(K)$. Accuracy of the obtained constants was evaluated by calculating the coefficient of determination, with an $R^2 > 0.98$ indicative of an acceptable fit. Due to the onset of Taylor–Couette instabilities, to estimate the high-shear viscosity, the viscosity curve was extrapolated and estimated data used to obtain $\mu_\infty = 9.1$ mPa s. This introduces considerable inconsistencies and is reported only to provide comparison to the high-shear viscosities reported in literature. Fig. 4a and b show the power-law fit of the developed shear-thinning blood analogue at 22 °C.

The shear-rate range used to determine the power-law fit is a compromise between the expected shear-rate *in-vitro* and the region where the data follows exponential behaviour. Larger fitting ranges can capture some of the plateau regions, decreasing the consistency index and reducing the coefficient of determination and overall fit quality. Conversely, smaller fitting ranges could result in a coefficient of determination approaching unity ($R^2 \rightarrow 1$) in the fitted region but reduced physiological relevancy if it is not representative of the expected shear rates.

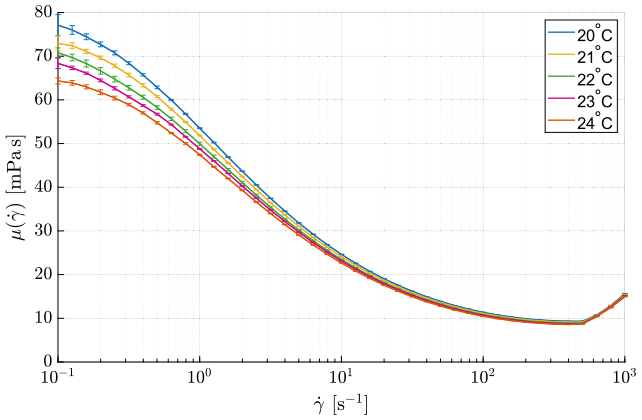


Fig. 3. Steady-shear sweep rheology of the non-Newtonian blood analogue ($n = 0.677$) measured at five temperatures (20−24 °C). Viscosity decreases with increasing shear rate, demonstrating pronounced shear-thinning. For a given shear rate, the apparent viscosity decreases with increasing temperature. Data exceeding $\dot{\gamma} \geq 500$ s^{-1} are affected by Taylor–Couette instabilities arising from the measurement geometry.

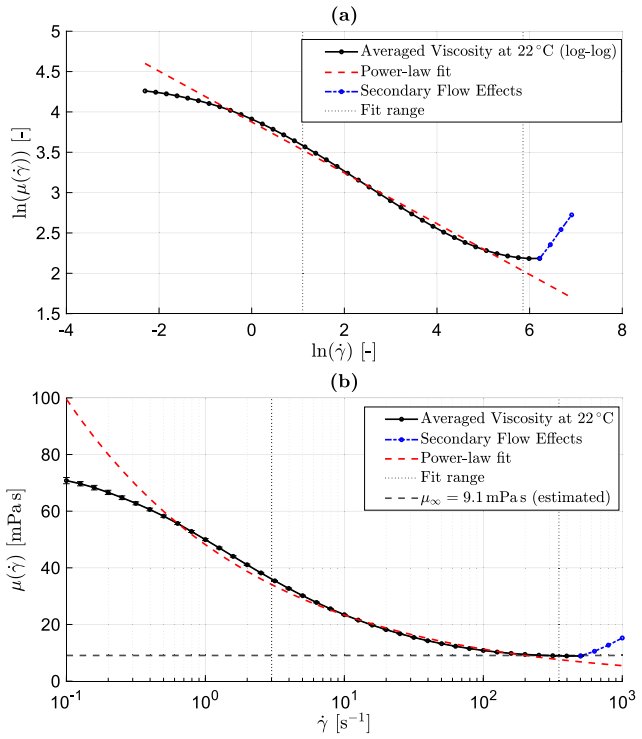


Fig. 4. (a) Log-Log representation of the steady-shear viscosity data at 22 °C with the corresponding power-law fit and fitting range used for parameter estimation. (b) Apparent viscosity as a function of shear rate and associated power-law fit. The estimated high-shear viscosity is also shown for comparison and highlights the limited applicability of Newtonian-based scaling for non-Newtonian fluids.

In this work, the final batch of fluid used for experimental measurements, achieved a power law index of $n = 0.677$ across a shear range of 1 $s^{-1} \leq \dot{\gamma} \leq$ 350 s^{-1} with 0.035% XG at 22 °C, matching the value for whole blood. However, the calculated consistency index of the developed analogue ($K = 49.77$ mPa s^n) significantly exceeded the reported values for blood and suggesting an overall higher viscosity for a given shear rate. Despite this, the validity of the blood analogue is not compromised because K is dimensional. Similarity is achieved by

Table 4
Variation of power-law constants with temperature in the developed blood analogue.

Temperature (°C)	n	K (mPa s^n)	R^2
20	0.674	52.860	0.992
21	0.676	51.408	0.992
22	0.677	49.770	0.993
23	0.678	48.825	0.993
24	0.680	47.599	0.993

matching the non-dimensional power-law index (n) and using the scaling equations incorporating K. To the authors' knowledge, this is the first time a low-viscosity, non-Newtonian blood analogue formulated using urea and XG was fitted to the power-law model.

The influence of temperature on the derived power-law parameters is given in Table 4. The same shear rate fitting range was used for all temperatures. The power law exponent increased with temperature indicating a decrease in shear-thinning while the consistency index displayed an inverse relationship. These parameter shifts can propagate into similitude equations and introduce measurement inaccuracies if overlooked, highlighting the need for frequent temperature monitoring for accurate replication of *in-vivo* conditions.

As previously discussed, despite following a starting constituent ratio when preparing an analogue fluid, it is necessary to tune the analogues RI to match that of a flow phantom ($\theta = 1.4124 \pm 0.0001$ at 22 °C) independently by altering constituent ratios. To evaluate formulation sensitivity and repeatability, two distinct series of solutions (Batch A and Batch B) were prepared using the same method and base ratio, and mixed using an identical manufacturer batch of XG. After mixing the Newtonian base, both fluids were tuned by adding small amounts of the base components until the fluid RI matched the phantom.

The influence of XG concentration on the derived power-law parameters, evaluated using triplicate rheological measurements (± 1 SD) of both fluids, is presented in Fig. 5. As little as 0.02% XG was seen to produce a power-law index (n) within the reported range in literature [9,55]. However, the physiological value is influenced by haematocrit, sample preparation and methodology. In this work 0.035% XG was selected for the separately prepared experimental batch (see Section 5.4) as it achieved the target power-law index ($n = 0.677$). Across all tested formulations, increasing XG concentration enhanced shear-thinning behaviour (decreasing n), while also increasing the consistency index (K).

While both batches exhibit similar qualitative trends, the slight compositional difference required for RI matching resulted in clear shifts in both power-law parameters for a given XG concentration. Despite Batch B having a slightly higher concentration of glycerol, it consistently displayed lower consistency indices (K), and higher power-law exponents (n) across all XG concentrations relative to Batch A. These differences highlight the sensitivity of the four-component fluid when RI matching is necessary. Further research is needed to determine the reasoning for this behaviour, and whether a specific component of the Newtonian base fluid effects XG behaviour, though this was beyond the scope of the present work. Small changes to the base concentration necessary for RI matching can cause considerable differences in measured non-Newtonian rheological properties. For all concentrations reported, the effect of XG on RI was negligible. It is however a key result that this variation exists, and therefore previous work that has relied on mixture ratios alone rather than testing each mixture will have likely not been obtaining the expected values. Both power-law parameters are extremely sensitive to XG concentration, and therefore rheological measurement of each analogue batch is necessary.

5.2.2. Oscillatory shear

The XG concentration used in this work is much higher than the optimal value reported by Brindise et al. [49] (0.02%), despite nearly identical Newtonian formulations. Their study did not include steady-shear measurements. Consequently, to enable meaningful comparison with the analogue and to demonstrate viscoelastic properties, oscillatory elasticity (ζ) and oscillatory viscosity (υ) were calculated from 2 Hz oscillatory measurements of the storage and loss modulus, using an identical frequency to Brindise et al. [49]. These parameters can be used to normalize both moduli and allow comparison across fluids with different densities or measurement frequencies.

$$\zeta = \frac{G'}{\omega\rho}, \qquad \upsilon = \frac{G''}{\omega\rho} \tag{7}$$

The strain-rate amplitude is defined as

$$\dot{\gamma}_0 = \gamma_0 \omega, \tag{8}$$

where γ_0 is the applied strain amplitude and $\omega = 2\pi f$ is the angular frequency. Fig. 6 shows the oscillatory viscosity and oscillatory elasticity of the developed analogue fluid in comparison to blood by Long et al. [81] and Thurston [22] and the reference 0.02% XG solution by Brindise et al. [49]. The developed blood analogue exhibits a similar decreasing trend in oscillatory elasticity with increasing strain rate, although with a greater reduction occurring at a lower strain rate than the 0.02% XG solution. This decline aligns with blood measurements reported by Thurston [22], although the overall magnitude slightly overestimates blood's elastic storage response.

For oscillatory viscosity, the developed analogue consistently exhibits a higher magnitude across all strain rates in comparison to blood and the reference analogue. This increase is attributed to the higher XG concentration needed to achieve the target power-law index necessary to achieve similitude, and also the slightly higher viscosity of the Newtonian base fluid. This supports findings that increased XG concentration increases oscillatory viscosity, though batch-to-batch variability of XG may also contribute to this finding [49,76]. While matching the

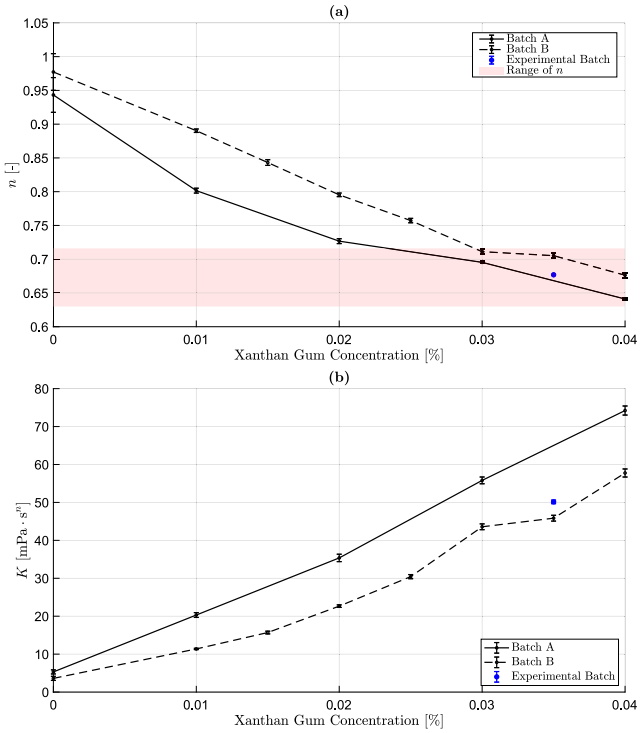


Fig. 5. (a) Change in the power-law exponent (n) with XG concentration of two RI-matched fluid batches and the experimental fluid used to obtain the non-Newtonian results in Section 5.4. The shaded region shows the range of n values reported in literature that should be matched to achieve similitude. (b) Change in the consistency index (K) with XG concentration.

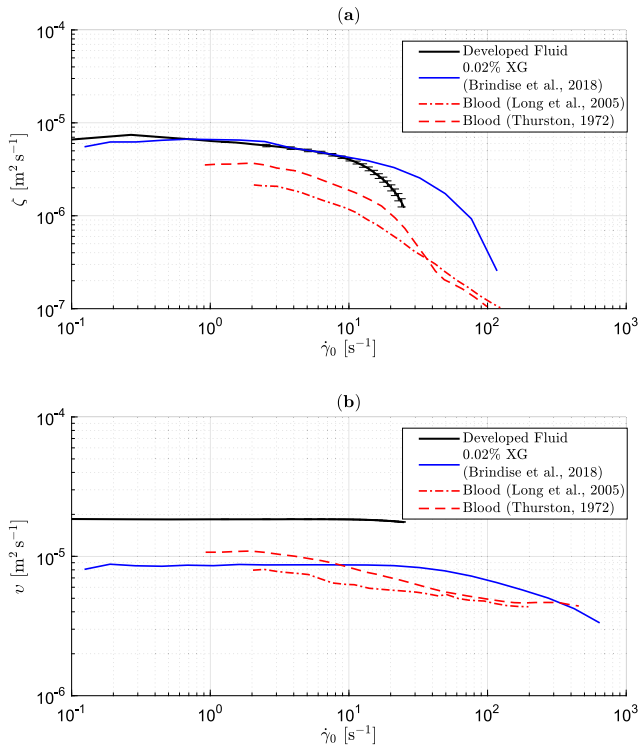


Fig. 6. (a) Oscillatory elasticity and (b) Oscillatory viscosity of the developed blood analogue fluid in comparison to measurements by Brindise et al. [49] with their low viscosity fluid and 0.02% XG, and blood data by Thurston [22] and Long et al. [81].

power-law index ensures shear-thinning behaviour is similar, it does not guarantee matched viscoelastic properties. Consequently, deviations in oscillatory response may influence results, especially under pulsatile flow conditions. However, as blood is weakly viscoelastic at low frequencies, this effect is likely small [16]. Nonetheless, while the analogue follows general qualitative viscoelastic trends, the difference in magnitude confirms that viscoelastic similitude has not been established in the present study. The scaling framework is restricted to the shear-thinning behaviour represented by the power-law model. Relaxation time and other measures of viscoelastic similitude were not matched or validated.

5.2.3. Density

Density measurements of the blood analogue were obtained at room temperature (22 ± 1 °C) using the average of several mass/volume measurements. Density of the non-Newtonian analogue was determined to be $1130 \pm 11.06\,\mathrm{kg\,m^{-3}}$. This is slightly higher than the density reported for blood, but similar to the density of the base solution reported by Brindise et al. [49] and still suitable for experimental analyses when employing similitude.

5.3. Application to physiological carotid waveform

To demonstrate the importance of considering non-Newtonian behaviour in scaling procedure, a physiological carotid artery inflow waveform is scaled using the parameters of the developed blood analogue. The waveform (Fig. 7a) was obtained previously from a healthy male volunteer [82,83] with a pulsation frequency of 1 Hz. The parameters used to scale the waveform are given in Table 5. To enable comparison, the *in-vitro* diameter and density were kept identical at $D = 17\,\mathrm{mm}$ and $\rho = 1130\,\mathrm{kg\,m^{-3}}$, respectively.

When the dynamic scaling procedure considering shear-dependent behaviour is employed, the waveform had a peak flowrate $Q = 144.59\,\mathrm{mL\,s^{-1}}$ compared to a peak flowrate of $Q = 98.95\,\mathrm{mL\,s^{-1}}$ when scaling the non-Newtonian analogue with μ_∞. This is a 46% increase in peak flow rate when considering non-Newtonian behaviour in scaling. The waveform time period also decreased by approximately 31% when shear-thinning was considered in scaling. These deviations in both flow rate and waveform frequency will have direct implications on the resulting haemodynamics by altering acceleration gradients, flow regimes, modifying WSS magnitude, and influencing the phase lag between pressure and velocity gradients. These differences strongly evidence that neglecting shear-dependent viscosity in the scaling procedure of non-Newtonian analogues may lead to experimental results that are not dynamically representative of the physiological system.

The choice of the *in-vivo* rheological parameters for blood could reduce or exaggerate the magnitude of the differences observed. Similarly, the choice of the shear range used to obtain the power-law constants could result in differences in this comparison. However, unlike scaling based on μ_∞, the power-law model explicitly incorporates shear-thinning behaviour, and therefore provides a scaling approach that is more consistent with the assumed non-Newtonian rheology of blood. The present comparison quantifies the resulting differences in prescribed flow conditions but does not independently validate their accuracy against physiological blood flow.

5.4. Experimental comparison in a carotid artery bifurcation phantom

Using the physiological carotid waveform defined in Section 5.3 the developed non-Newtonian power-law blood analogue (0.035% XG, experimental batch) and a Newtonian reference fluid were compared experimentally using Planar-PIV. A compliant carotid bifurcation (CAB) phantom manufactured in-house from SYLGARD 184 with a common carotid artery (CCA) inlet diameter of 17 mm was utilized. The Newtonian fluid was formulated using the base ratio outlined in Section 5, before being tuned to match the RI of the phantom and characterized. The Newtonian flow was then scaled using the Newtonian Re and α, assuming blood with an asymptotic viscosity value of $\mu_\infty = 3.5\,\mathrm{mPa\,s}$. Meanwhile, the power-law blood analogue was scaled using Re_{PL} and St as presented in Section 5.3.

The phantom was attached to a flow circuit which imposed a pulsatile inlet condition using a ViVitro Superpump (ViVitro Labs Inc., Victoria, BC) and steady flow centrifugal pump arranged in parallel. Both fluids were seeded with hollow glass spheres with a nominal diameter 9 µm to 13 µm. A total of 50 image pairs were obtained at peak systole using a LaVision Flowmaster PIV system (LaVision GmbH, Germany) was used to capture the flow, illuminated with an Nd:YAG laser (Litron Nano S 65-15 PIV). Images were pre-processed and velocity vectors calculated using cross-correlation in LaVision DaVis (10.2.1). The vector fields were then ensemble-averaged and spurious vectors removed. To enable physiologically relevant comparisons, velocity fields were rescaled to *in-vivo* scale and presented using MATLAB (R2025, Mathworks, USA).

Fig. 8 presents the ensemble-averaged velocity fields and streamlines in the carotid bifurcation at peak systole with the Newtonian analogue (Fig. 8a) and the non-Newtonian analogue (Fig. 8b). Both analogue fluids exhibit qualitative similarities in flow behaviour. This includes high velocity jet entering the CCA, shifting towards the outer wall as it progresses downstream due to the curvature and a low velocity region on the outer walls of both daughter branches.

In the CCA branch however, the core flow velocity in the Newtonian case had a higher magnitude, reflecting the reduction in peak velocity as a direct result of shear-thinning effects non-Newtonian case. This behaviour propagated into greater differences between the two fluids in the daughter branches. For example, a small flow separation was established along the inner wall of the internal carotid artery (ICA, left) in both cases, however the separation was significantly larger in the non-Newtonian case. Here, the area with velocity $|U| < 0.2\,\mathrm{m\,s^{-1}}$, was $2.51\,\mathrm{mm^2}$ in the Newtonian case and $5.14\,\mathrm{mm^2}$ in the non-Newtonian

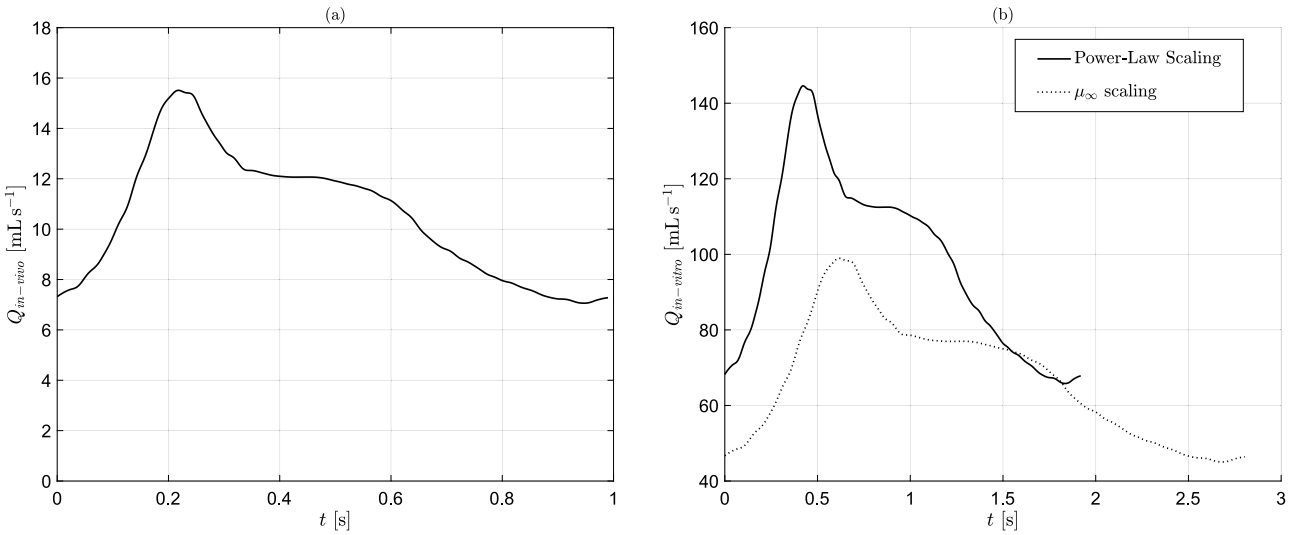


Fig. 7. (a) *In-vivo* flowrate waveform at the inlet of the carotid artery bifurcation. (b) Comparison of the associated experimental waveforms when using the non-Newtonian blood analogue and scaling inlet conditions using the Newtonian scaling (Re and α) method with μ_∞, or the power-law method (Re_{PL}, St, n, and $\frac{\bar{u}}{\bar{u}}$).

Table 5
Parameters used to scale the carotid waveform in Fig. 7a, dimensionless numbers were preserved between *in-vivo* and *in-vitro* systems, with identical diameters for the blood analogue to enable comparison between methods.

	In-vivo	Newtonian scaling (μ_∞)	Power-law scaling
Diameter, D [mm]	6.5	17	17
Average flowrate, $\bar{Q}$ [mL s^{-1}]	10.51	67.06	98.00
Time period, t [s]	1	2.80	1.92
Density, ρ [kg m^{-3}]	1060	1130	1130
High-shear viscosity, μ_∞ [mPa s]	3.5	9.1	–
Power-Law exponent, n [–]	0.677	–	0.677
Consistency index, K, [mPa s^n]	16.2	–	49.77
Strouhal number, St [–]	0.13	0.13	0.13
Womersley number, α [–]	4.48	4.48	–
Average Newtonian Reynolds number, Re_N [–]	624	624	–
Average generalized Reynolds number, Re_{PL} [–]	479	–	479

case. This may be caused by the differing jet entry angles and branch flow division due to shear-thinning effects. Along the outer wall of both branches, the low velocity region also exhibited stark differences, with a smaller area of low velocity flow in the Newtonian case.

The observed differences in flow distribution demonstrate the influence of incorporating shear-thinning rheology together with the corresponding power-law scaling strategy, including changes in downstream flow distribution, separation and velocity profile development. These findings demonstrate that the choice of rheological representation and scaling approach can materially alter the experimentally measured haemodynamic field. However, the PIV measurements compare two analogue fluid approaches within the same phantom and do not provide a direct experimental validation against physiological blood flow. The results should therefore be interpreted as a demonstration of the consequences of rheology and scaling choice.

6. Conclusion and future recommendations

Blood exhibits several complex rheological behaviours including shear-thinning and viscoelasticity. Accurate modelling of blood and blood flow is necessary for both vascular research and pre-clinical testing of medical devices. Due to challenges in the creation of a non-Newtonian blood analogue, a Newtonian approximation is commonly used in *in-vitro* experiments, yet recent computational and experimental studies have suggested this assumption may lead to notably different haemodynamic fields, reducing clinical relevancy. This work therefore outlines the limitations of existing Newtonian and non-Newtonian blood analogues and presents the development and characterization of an RI-matched, shear-thinning blood analogue suitable for optical flow measurements highlighting the steps taken to address these limitations.

Newtonian analogues are typically derived from aqueous glycerol, with an optional third component to enable RI tuning whilst maintaining a physiologically similar viscosity. Salts like NaI have been used as a third component, however they are limited by safety constraints. Two safer alternatives are urea or xylitol, with urea in particular enabling RI tuning with minimal influence on density and viscous properties compared to salt-based solutions.

Shear-thinning and viscoelastic behaviour can be induced by adding small amounts of polymers to the Newtonian formulations. XG has been implemented in various concentrations in contrast to other polymers given its improved elastic properties and solubility over PAA and nylon. However, implementation of XG is not straightforward, and every fluid batch requires rheological characterization to confirm physiological relevancy. Inter- and intra-manufacturer XG batch differences have been shown to influence both shear-thinning and elastic properties. Additionally salt concentration, fluid temperature and pH can alter the rheological significantly and rapidly due to structural changes of XG molecules.

Although the use of non-Newtonian blood analogues is becoming more common in experimental studies, many works omit scaling methodology or rely on dimensionless numbers that are calculated from the high-shear viscosity such as the Newtonian Reynolds number and the Womersley number, which do not account for shear-thinning behaviour. Neglecting this in similitude formulae can introduce error

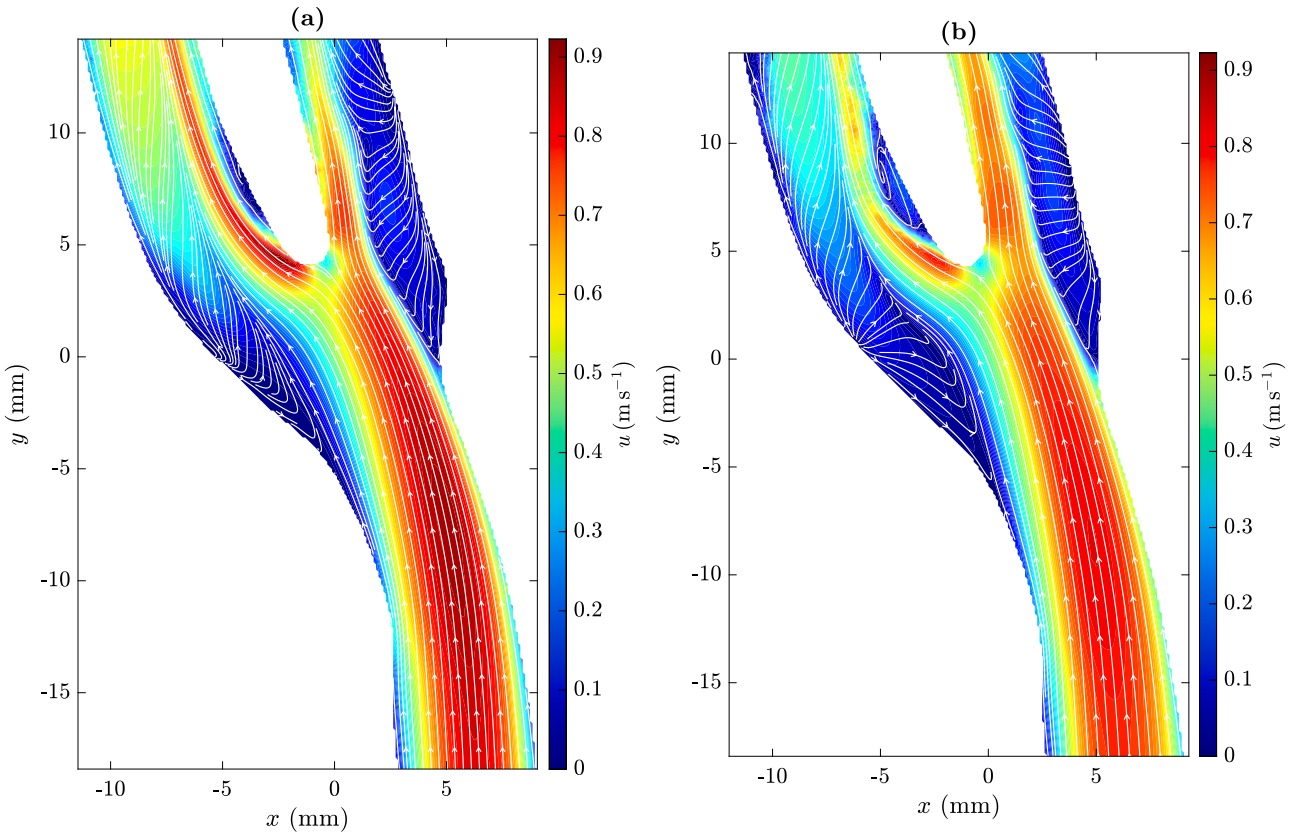


Fig. 8. (a) Velocity distribution and streamlines of the CAB at peak systole with the Newtonian fluid. (b) Velocity distribution and streamlines of the CAB at peak systole with the non-Newtonian power-law fluid, scaled using Re_{PL} and St.

and reduce clinical relevance. To address this, accurate dynamic scaling of shear-dependent fluids like blood requires the incorporation of a constitutive rheological model during dimensional analysis and the matching of parameters such as the power-law index and the generalized Reynolds number between systems. This approach has only been reported in the previous haemodynamic study by Gray et al. [9] and hence remains largely overlooked in the field despite being vital to ensure similarity of non-Newtonian, pulsatile flows.

The developed blood analogue comprised of water, glycerol, urea and XG and was characterized with both steady-shear and oscillatory rheological measurements across a range of temperatures. The degree of shear-thinning and fluid consistency were seen to decrease with increasing temperature. An increase in XG concentration resulted in an increase in shear-thinning behaviour. Oscillatory measurements showed qualitatively similar trends in elastic response, although differences in magnitude were observed and viscoelastic similitude was not established. The oscillatory viscosity was also higher in the developed analogue, likely due to the additional XG required to match the target power-law index. This work demonstrates that rheological properties of XG-based blood analogues cannot be assumed and vary with temperature, concentration, and batch. Experimentalists should not rely on pre-defined ratios from literature and assume identical properties. Frequent monitoring and batch-specific rheological characterization are essential to ensure analogue stability and ensure physiological relevance in haemodynamic experiments.

A PIV comparison of two flows in a CAB geometry with Newtonian and non-Newtonian analogues demonstrated measurable differences associated with the rheological representation and corresponding scaling approach. At peak systole, altered flow distribution and dampening of the peak inlet velocity was observed in the non-Newtonian case suggesting that neglecting the shear-thinning characteristics of whole blood in haemodynamic measurements could result in misinterpretations of key haemodynamic metrics.

Future *in-vitro* studies utilizing a non-Newtonian blood analogue with XG should perform rigorous characterization of fluid rheology to maintain physiological relevancy by conducting both steady-shear and oscillatory measurements to ensure that both the shear-thinning and viscoelastic properties are suitable. Dynamic scaling of flow conditions should consider shear-dependent behaviour by incorporating constitutive models like the power-law model. Accurate temperature control is needed to ensure the analogue maintains relevancy during measurements and for extended experiments, regular characterization, along with RI monitoring is required to ensure fluid longevity and prevent degradation. The validity of experimental studies employing non-Newtonian blood analogues should be critically assessed if rheological data and scaling methodologies are unreported, as these are fundamental to ensuring physiological relevance.

CRediT authorship contribution statement

J.A. Lowe: Writing – original draft, Visualization, Methodology, Investigation, Formal analysis, Conceptualization. **E.P.F. Barton:** Investigation, Formal analysis. **R.L. Lewis:** Investigation, Formal analysis. **J.-B.R.G. Souppez:** Writing – review & editing, Supervision. **W.H. Ho:** Writing – review & editing, Supervision. **S.G. Yazdi:** Supervision. **L.J. Leslie:** Writing – review & editing, Supervision. **P.T. Griffiths:** Writing – review & editing. **P.H. Geoghegan:** Writing – review & editing, Supervision, Conceptualization.

Declaration of competing interest

The authors declare that they have no known competing financial interests or personal relationships that could have appeared to influence the work reported in this paper.

Acknowledgements

This work is supported by UKRI - EPSRC Doctoral Training Program (grant EPSRC DTP EP/T518128/1) & Aston University. The authors would also like to acknowledge the technical staff at Aston University for their support.

Data availability

Data will be made available on request.

References

[1] M. Bonfanti, G. Franzetti, S. Homer-Vanniasinkam, V. Diaz-Zuccarini, S. Balabani, A combined in vivo, in vitro, in silico approach for Patient-Specific haemodynamic studies of Aortic dissection, Ann. Biomed. Eng. 48 (12) (2020) 2950–2964, http://dx.doi.org/10.1007/s10439-020-02603-z.

[2] ASME V&V 40, Assessing Credibility of Computational Modeling through Verification and Validation: Application to Medical Devices, The American Society of Mechanical Engineers, New York, NY, 2018.

[3] J. Romberg, K. Srikantharajah, J. Brüning, J.R. Rangarajan, Devices Approval Experience Report, Technical Report Deliverable 9.6, SIMCor; BIOTRONIK, 2024, Grant Agreement No. 101017578; H2020-SC1-DTH-2018-2020.

[4] A. Zaman, N. Ali, M. Sajid, T. Hayat, Effects of unsteadiness and non-Newtonian rheology on blood flow through a tapered time-variant stenotic artery, AIP Adv. 5 (3) (2015) 037129, http://dx.doi.org/10.1063/1.4916043.

[5] P.H. Geoghegan, M.C. Jermy, D.S. Nobes, A piv comparison of the flow field and wall shear stress in rigid and compliant models of healthy carotid arteries, J. Mech. Med. Biol. 17 (03) (2016) http://dx.doi.org/10.1142/s0219519417500415.

[6] D.N. Ku, BLOOD FLOW IN ARTERIES, Annu. Rev. Fluid Mech. 29 (1) (1997) 399–434, http://dx.doi.org/10.1146/annurev.fluid.29.1.399.

[7] S.G. Yazdi, P.H. Geoghegan, P.D. Docherty, M. Jermy, A. Khanafer, A review of Arterial Phantom fabrication methods for flow measurement using PIV techniques, Ann. Biomed. Eng.: J. Biomed. Eng. Soc. 46 (11) (2018) 1697, http://dx.doi.org/10.1007/s10439-018-2085-8.

[8] A.L. Cheng, N.M. Pahlevan, D.G. Rinderknecht, J.C. Wood, M. Gharib, Experimental investigation of the effect of non-Newtonian behavior of blood flow in the Fontan circulation, Eur. J. Mech. B Fluids 68 (2018) 184–192, http://dx.doi.org/10.1016/j.euromechflu.2017.12.009, URL: https://www.sciencedirect.com/science/article/pii/S099775461730417X.

[9] J.D. Gray, I. Owen, M.P. Escudier, Dynamic scaling of unsteady shear-thinning non-Newtonian fluid flows in a large-scale model of a distal anastomosis, Exp. Fluids 43 (4) (2007) 535–546, http://dx.doi.org/10.1007/s00348-007-0317-z.

[10] M. Samaee, A. Nooraeen, M. Tafazzoli-Shadpour, H. Taghizadeh, A comparison of Newtonian and non-Newtonian pulsatile blood rheology in carotid bifurcation through fluid–solid interaction hemodynamic assessment based on experimental data, Phys. Fluids 34 (7) (2022) 071902, http://dx.doi.org/10.1063/5.0094656.

[11] J. Xiang, M. Tremmel, J. Kolega, E.I. Levy, S.K. Natarajan, H. Meng, Newtonian viscosity model could overestimate wall shear stress in intracranial aneurysm domes and underestimate rupture risk, J. NeuroInterventional Surg. 4 (5) (2012) 351–357, http://dx.doi.org/10.1136/neurintsurg-2011-010089, URL: https://jnis.bmj.com/content/4/5/351, Publisher: British Medical Journal Publishing Group Section: Hemorrhagic stroke.

[12] V. Thondapu, D. Shishikura, J. Dijkstra, S.J. Zhu, E. Revalor, P.W. Serruys, W.J. van Gaal, E.K.W. Poon, A. Ooi, P. Barlis, Non-Newtonian endothelial shear stress simulation: Does it matter? Front. Cardiovasc. Med. 9 (2022) 835270, http://dx.doi.org/10.3389/fcvm.2022.835270, URL: https://www.ncbi.nlm.nih.gov/pmc/articles/PMC9046559/.

[13] C.G. Caro, T.J. Pedley, R.C. Schroter, W.A. Seed, K.H. Parker, The mechanics of the circulation, second ed., Cambridge University Press, 2012.

[14] H.A. Barnes, The yield stress—a review or 'panta rhei' —everything flows? J. Non-Newton. Fluid Mech. 81 (1) (1999) 133–178, http://dx.doi.org/10.1016/S0377-0257(98)00094-9, URL: https://www.sciencedirect.com/science/article/pii/S0377025798000949.

[15] G. Thurston, Viscoelasticity of human blood, Biophys. J. 12 (9) (1972) 1205–1217, http://dx.doi.org/10.1016/S0006-3495(72)86156-3, Publisher: Elsevier.

[16] L. Campo-Deaño, R.P.A. Dullens, D.G.A.L. Aarts, F.T. Pinho, M.S.N. Oliveira, Viscoelasticity of blood and viscoelastic blood analogues for use in polydymethylsiloxane in vitro models of the circulatory system, Biomicrofluidics 7 (3) (2013) 34102, http://dx.doi.org/10.1063/1.4804649.

[17] A.N. Beris, J.S. Horner, S. Jariwala, M.J. Armstrong, N.J. Wagner, Recent advances in blood rheology: a review, Soft Matter 17 (47) (2021) 10591–10613, http://dx.doi.org/10.1039/D1SM01212F, URL: https://pubs.rsc.org/en/content/articlelanding/2021/sm/d1sm01212f, Publisher: The Royal Society of Chemistry.

[18] W.H. Bauer, E.A. Collins, Chapter 8 - thixotropy and dilatancy, in: F.R. Eirich (Ed.), Rheology, Academic Press, 1967, pp. 423–459, http://dx.doi.org/10.1016/B978-1-4832-2941-6.50014-3, URL: https://www.sciencedirect.com/science/article/pii/B9781483229416500143.

[19] A.M. Robertson, A. Sequeira, R.G. Owens, Rheological models for blood, in: L. Formaggia, A. Quarteroni, A. Veneziani (Eds.), Cardiovascular Mathematics: Modeling and Simulation of the Circulatory System, Springer Milan, Milano, 2009, pp. 211–241, http://dx.doi.org/10.1007/978-88-470-1152-6_6.

[20] N. Bessonov, A. Sequeira, S. Simakov, Y. Vassilevskii, V. Volpert, Methods of blood flow modelling, Math. Model. Nat. Phenom. 11 (1) (2016) 1–25, http://dx.doi.org/10.1051/mmnp/201611101, URL: https://www.mmnp-journal.org/articles/mmnp/abs/2016/01/mmnp2016111p1/mmnp2016111p1.html, Number: 1 Publisher: EDP Sciences.

[21] E. Nader, S. Skinner, M. Romana, R. Fort, N. Lemonne, N. Guillot, A. Gauthier, S. Antoine-Jonville, C. Renoux, M.-D. Hardy-Dessources, E. Stauffer, P. Joly, Y. Bertrand, P. Connes, Blood rheology: Key parameters, impact on blood flow, role in sickle cell disease and effects of exercise, Front. Physiol. 10 (2019) 1329, http://dx.doi.org/10.3389/fphys.2019.01329, URL: https://www.ncbi.nlm.nih.gov/pmc/articles/PMC6842957/.

[22] G.B. Thurston, Effects of viscoelasticity of blood on wave propagation in the circulation, J. Biomech. 9 (1) (1976) 13–20, http://dx.doi.org/10.1016/0021-9290(76)90134-2, URL: https://www.sciencedirect.com/science/article/pii/0021929076901342.

[23] A.J. Apostolidis, A.N. Beris, The effect of cholesterol and triglycerides on the steady state shear rheology of blood, Rheol. Acta 55 (6) (2016) 497–509, http://dx.doi.org/10.1007/s00397-015-0889-0.

[24] I. Ebenuwa, P.-C. Violet, H. Tu, C. Lee, N. Munyan, Y. Wang, M. Niyyati, K. Patra, K.J. Wilkins, N. Parrow, M. Levine, Altered RBC deformability in diabetes: clinical characteristics and RBC pathophysiology, Cardiovasc. Diabetol. 23 (1) (2024) 370, http://dx.doi.org/10.1186/s12933-024-02453-2.

[25] V. Kannojiya, A.K. Das, P.K. Das, Simulation of blood as fluid: A review from rheological aspects, IEEE Rev. Biomed. Eng. 14 (2021) 327–341, http://dx.doi.org/10.1109/RBME.2020.3011182, URL: https://ieeexplore.ieee.org/abstract/document/9146357?casa_token=tu5AQcUxKSAAAAAA:o6eQjyCFJBLJwmYqe64hxGLKMzXjIG6-xuD98boP4KkNupYl06xLu-gQlAqKPzeqsMbO8OIhc3c, Conference Name: IEEE Reviews in Biomedical Engineering.

[26] C. Abugattas, A. Aguirre, E. Castillo, M. Cruchaga, Numerical study of bifurcation blood flows using three different non-Newtonian constitutive models, Appl. Math. Model. 88 (2020) 529–549, http://dx.doi.org/10.1016/j.apm.2020.06.066, URL: https://www.sciencedirect.com/science/article/pii/S0307904X20303425.

[27] N. Sarkar, S.D. Sharma, S. Chakraborty, S. Roy, A comparative study of Newtonian and non-Newtonian blood flow through Bi-Leaflet mechanical heart valve, Comput. & Fluids 279 (2024) 106337, http://dx.doi.org/10.1016/j.compfluid.2024.106337, URL: https://www.sciencedirect.com/science/article/pii/S0045793024001695.

[28] H. Yi, Z. Yang, M. Johnson, L. Bramlage, B. Ludwig, Hemodynamic characteristics in a cerebral aneurysm model using non-Newtonian blood analogues, Phys. Fluids 34 (10) (2022) 103101, http://dx.doi.org/10.1063/5.0118097.

[29] J. Chen, X.-Y. Lu, Numerical investigation of the non-Newtonian blood flow in a bifurcation model with a non-planar branch, J. Biomech. 37 (12) (2004) 1899–1911, http://dx.doi.org/10.1016/j.jbiomech.2004.02.030, URL: https://www.sciencedirect.com/science/article/pii/S0021929004001198.

[30] H.W. Choi, A.I. Barakat, Numerical study of the impact of non-Newtonian blood behavior on flow over a two-dimensional backward facing step, Biorheology 42 (6) (2005) 493–509.

[31] Y.-T. Liu, Z.-M.-Y. Zhang, M.-L. Li, S. Gao, F. Feng, W.-H. Xu, Association of carotid artery geometries with middle cerebral artery atherosclerosis, Atherosclerosis 352 (2022) 27–34, http://dx.doi.org/10.1016/j.atherosclerosis.2022.05.016.

[32] G. Fragomeni, Newtonian and non-Newtonian blood model, a comparative study on large and small vessels, in: Proceedings of the 12th International Workshop on Innovative Simulation for Healthcare, IWISH, CAL-TEK srl, 2023, http://dx.doi.org/10.46354/i3m.2023.iwish.007, URL: https://www.cal-tek.eu/proceedings/i3m/2023/iwish/007.

[33] A.C. Stamou, J. Radulovic, J.M. Buick, A comparison of Newtonian and Non-Newtonian models for simulating Stenosis development at the bifurcation of the Carotid Artery, Fluids 8 (10) (2023) 282, http://dx.doi.org/10.3390/fluids8100282, URL: https://www.mdpi.com/2311-5521/8/10/282.

[34] D. Biswas, D.M. Casey, D.C. Crowder, D.A. Steinman, Y.H. Yun, F. Loth, Characterization of transition to turbulence for blood in a straight pipe under steady flow conditions, J. Biomech. Eng. 138 (7) (2016).

[35] A.D. Anastasiou, A.S. Spyrogianni, K.C. Koskinas, G.D. Giannoglou, S.V. Paras, Experimental investigation of the flow of a blood analogue fluid in a replica of a bifurcated small artery, Med. Eng. Phys. 34 (2) (2012) 211–218, http://dx.doi.org/10.1016/j.medengphy.2011.07.012, URL: https://www.sciencedirect.com/science/article/pii/S135045331100169X.

[36] V. Deplano, Y. Knapp, L. Bailly, E. Bertrand, Flow of a blood analogue fluid in a compliant abdominal aortic aneurysm model: experimental modelling, J. Biomech. 47 (6) (2014) 1262–1269, http://dx.doi.org/10.1016/j.jbiomech.2014.02.026.

[37] S. Frolov, S. Sindeev, D. Liepsch, A. Balasso, Experimental and CFD flow studies in an intracranial aneurysm model with Newtonian and non-Newtonian fluids, Technol. Health Care 24 (3) (2016) 317–333, http://dx.doi.org/10.3233/THC-161132, URL: https://journals.sagepub.com/action/showAbstract, Publisher: SAGE Publications.

[38] M.S. Zakaria, S. Zainudin, H. Abdullah, C. Yuan, M. Abd Latif, A. Latif, K. Osman, F. Mekanikal, CFD simulation of Non-Newtonian effect on hemodynamics characteristics of blood flow through benchmark nozzle, J. Adv. Res. FluidMechanics Therm. Sci. 64 (1) (2019) 117–125.

[39] S. Lynch, N. Nama, C.A. Figueroa, Effects of non-Newtonian viscosity on arterial and venous flow and transport, Sci. Rep. 12 (1) (2022) 20568, http://dx.doi.org/10.1038/s41598-022-19867-1, URL: https://www.nature.com/articles/s41598-022-19867-1.

[40] A. Chauhan, C. Sasmal, The influence of non-Newtonian behaviors of blood on the hemodynamics past a bileaflet mechanical heart valve, Phys. Fluids 36 (10) (2024) 101918, http://dx.doi.org/10.1063/5.0231839.

[41] D. Jasikova, N. Pluchova, M. Kotek, V. Kopecký, Evaluation of the influence of anomalies on the flow of non-Newtonian fluid in carotid bifurcation by the PIV method, MATEC Web Conf. 328 (2020) 05005, http://dx.doi.org/10.1051/matecconf/202032805005, URL: https://www.matec-conferences.org/articles/matecconf/abs/2020/24/matecconf_aenmfme2020_05005/matecconf_aenmfme2020_05005.html, Publisher: EDP Sciences.

[42] A.L. DiCarlo, D.W. Holdsworth, T.L. Poepping, Study of the effect of stenosis severity and non-Newtonian viscosity on multidirectional wall shear stress and flow disturbances in the carotid artery using particle image velocimetry, Med. Eng. Phys. 65 (2019) 8–23, http://dx.doi.org/10.1016/j.medengphy.2018.12.023.

[43] H.K. Huh, H. Ha, S.J. Lee, Effect of non-Newtonian viscosity on the fluid-dynamic characteristics in stenotic vessels, Exp. Fluids 56 (8) (2015) 167, http://dx.doi.org/10.1007/s00348-015-2037-0.

[44] C. Completo, V. Geraldes, V. Semiao, Rheological and dynamical characterization of blood analogue flows in a slit, Int. J. Heat Fluid Flow 46 (2014) 17–28, http://dx.doi.org/10.1016/j.ijheatfluidflow.2013.12.008, URL: https://www.sciencedirect.com/science/article/pii/S0142727X1300249X.

[45] V. Deplano, Y. Knapp, E. Bertrand, E. Gaillard, Flow behaviour in an asymmetric compliant experimental model for abdominal aortic aneurysm, J. Biomech. 40 (11) (2007) 2406–2413, http://dx.doi.org/10.1016/j.jbiomech.2006.11.017.

[46] A.M. Walker, C.R. Johnston, D.E. Rival, On the characterization of a non-Newtonian blood analog and its response to pulsatile flow downstream of a simplified stenosis, Ann. Biomed. Eng. 42 (1) (2014) 97–109, http://dx.doi.org/10.1007/s10439-013-0893-4.

[47] F.J.H. Gijsen, F.N. van de Vosse, J.D. Janssen, The influence of the non-Newtonian properties of blood on the flow in large arteries: steady flow in a carotid bifurcation model, J. Biomech. 32 (6) (1999) 601–608, http://dx.doi.org/10.1016/S0021-9290(99)00015-9.

[48] P.H. Geoghegan, N.A. Buchmann, C.J.T. Spence, S. Moore, M. Jermy, Fabrication of rigid and flexible refractive-index-matched flow phantoms for flow visualisation and optical flow measurements, Exp. Fluids 52 (5) (2012) 1331–1347, http://dx.doi.org/10.1007/s00348-011-1258-0.

[49] M.C. Brindise, M.M. Busse, P.P. Vlachos, Density and viscosity matched Newtonian and non-Newtonian Blood-Analog solutions with PDMS refractive index, Exp. Fluids 59 (11) (2018) http://dx.doi.org/10.1007/s00348-018-2629-6.

[50] E. Hosseinzadeh, H. Mirgolbabaee, L. Van De Velde, M. Versluis, E. Groot Jebbink, A. Aguirre-Soto, M.M.P.J. Reijnen, Soft stereolithographic 3D printed phantoms for dual-modality particle image velocimetry (PIV), Exp. Fluids 66 (1) (2025) 20, http://dx.doi.org/10.1007/s00348-024-03938-2, URL: https://link.springer.com/10.1007/s00348-024-03938-2.

[51] W.H. Ho, I.J. Tshimanga, M.N. Ngoepe, M.C. Jermy, P.H. Geoghegan, Evaluation of a desktop 3D printed rigid refractive-indexed-matched flow phantom for PIV measurements on cerebral aneurysms, Cardiovasc. Eng. Technol. 11 (1) (2020) 14–23, http://dx.doi.org/10.1007/s13239-019-00444-z.

[52] K. Jędrzejczak, A. Antonowicz, B. Butruk-Raszeja, W. Orciuch, K. Wojtas, P. Piasecki, J. Narloch, M. Wierzbicki, Ł. Makowski, Three-dimensionally printed elastic cardiovascular phantoms for carotid angioplasty training and personalized healthcare, J. Clin. Med. 13 (17) (2024) 5115, http://dx.doi.org/10.3390/jcm13175115, URL: https://www.mdpi.com/2077-0383/13/17/5115, Publisher: Multidisciplinary Digital Publishing Institute.

[53] B. Ngatane, J.A. Dicks, W.H. Ho, M. Ngoepe, Masked stereolithography as an accessible additive manufacturing technology to fabricate soft polymeric flow phantoms, MATEC Web Conf. 406 (2024) 07014, http://dx.doi.org/10.1051/matecconf/202440607014, URL: https://www.matec-conferences.org/articles/matecconf/abs/2024/18/matecconf_rapdasa2024_07014/matecconf_rapdasa2024_07014.html, Publisher: EDP Sciences.

[54] M.A. Elblbesy, B.A. Kandil, M.A. Elblbesy, B.A. Kandil, Hemorheological measurements over the shear-thinning regime. In vitro comparative study for hyperglycemia, AIMS Biophys. 11 (2) (2024) 121–129, http://dx.doi.org/10.3934/biophy.2024008, URL: http://www.aimspress.com/article/doi/10.3934/biophy.2024008, Cc_license_type: cc_by Number: biophy-11-02-008 Primary_atype: AIMS Biophysics Subject_term: Research article Subject_term_id: Research article.

[55] C. Trejo-Soto, A. Hernández-Machado, Normalization of blood viscosity according to the hematocrit and the shear rate, Micromachines 13 (3) (2022) 357, http://dx.doi.org/10.3390/mi13030357, URL: https://www.mdpi.com/2072-666X/13/3/357, Number: 3 Publisher: Multidisciplinary Digital Publishing Institute.

[56] M. Elblbesy, A. Hereba, Computation of the coefficients of the power law model for whole blood and their correlation with blood parameters, J. Appl. Phys. Res. 8 (2) (2016) http://dx.doi.org/10.5539/apr.v8n2p1.

[57] M. Karsheva, P. Dinkova, I. Pentchev, T. Ivanova, Blood rheology-a key for blood circulation in human body, J. Univ. Chem. Technol. Met. 44 (1) (2009) 50–54.

[58] M.A. Hussain, S. Kar, R.R. Puniyani, Relationship between power law coefficients and major blood constituents affecting the whole blood viscosity, J. Biosci. 24 (1999) 329–337, ISBN: 0250-5991 Publisher: Springer.

[59] A. Hussain, R. Puniyani, S. Kar, Quantification of blood viscosity using power law model in cerebrovascular accidents and high risk controls, Clin. Hemorheol. Microcirc. 14 (5) (1994) 685–696, http://dx.doi.org/10.3233/CH-1994-14507, URL: https://journals.sagepub.com/action/showAbstract, Publisher: SAGE Publications.

[60] M.Y. Yousif, D.W. Holdsworth, T.L. Poepping, A blood-mimicking fluid for particle image velocimetry with silicone vascular models, Exp. Fluids 50 (3) (2010) 769–774, http://dx.doi.org/10.1007/s00348-010-0958-1.

[61] M.R. Najjari, J.A. Hinke, K.V. Bulusu, M.W. Plesniak, On the rheology of refractive-index-matched, non-Newtonian blood-analog fluids for PIV experiments, Exp. Fluids 57 (6) (2016) http://dx.doi.org/10.1007/s00348-016-2185-x.

[62] T.J. Snoeijink, J.L. van der Hoek, H. Mirgolbabaee, T.G. Vlogman, J. Roosen, J.F.W. Nijsen, E. Groot Jebbink, In vitro investigation of microcatheter behavior during microsphere injection in transarterial radioembolization, J. Endovasc. Ther. (2025) 15266028251318953, http://dx.doi.org/10.1177/15266028251318953, Publisher: SAGE Publications Inc.

[63] M.L. Tomov, L. Perez, L. Ning, H. Chen, B. Jing, A. Mingee, S. Ibrahim, A.S. Theus, G. Kabboul, K. Do, S.R. Bhamidipati, J. Fischbach, K. McCoy, B.A. Zambrano, J. Zhang, R. Avazmohammadi, A. Mantalaris, B.D. Lindsey, D. Frakes, L.P. Dasi, V. Serpooshan, H. Bauser-Heaton, A 3D bioprinted in vitro model of pulmonary artery atresia to evaluate endothelial cell response to microenvironment, Adv. Healthc. Mater. 10 (20) (2021) 2100968, http://dx.doi.org/10.1002/adhm.202100968, URL: https://onlinelibrary.wiley.com/doi/abs/10.1002/adhm.202100968, _eprint: https://onlinelibrary.wiley.com/doi/pdf/10.1002/adhm.202100968.

[64] A. Shuib, P. Hoskins, W. Easson, Experimental investigation of particle distribution in a flow through a stenosed artery, J. Mech. Sci. Technol. 25 (2) (2011) 357–364, http://dx.doi.org/10.1007/s12206-010-1232-4.

[65] T.T. Nguyen, Y. Biadillah, R. Mongrain, J. Brunette, J.-C. Tardif, O.F. Bertrand, A method for matching the refractive index and kinematic viscosity of a blood analog for flow visualization in hydraulic cardiovascular models, J. Biomech. Eng. 126 (4) (2004) 529–535, http://dx.doi.org/10.1115/1.1785812.

[66] E. Doutel, N. Viriato, J. Carneiro, J.B. Campos, J.M. Miranda, Geometrical effects in the hemodynamics of stenotic and non-stenotic left coronary arteries—numerical and in vitro approaches, Int. J. Numer. Methods Biomed. Eng. 35 (8) (2019) e3207, http://dx.doi.org/10.1002/cnm.3207, URL: https://onlinelibrary.wiley.com/doi/abs/10.1002/cnm.3207.

[67] V. Carvalho, N. Rodrigues, R. Ribeiro, P.F. Costa, R.A. Lima, S. F. C.F. Teixeira, 3D printed biomodels for flow visualization in stenotic vessels: An experimental and numerical study, Micromachines 11 (6) (2020) 549, http://dx.doi.org/10.3390/mi11060549, URL: https://www.mdpi.com/2072-666X/11/6/549, Publisher: Multidisciplinary Digital Publishing Institute.

[68] J. Clauser, M.S. Knieps, M. Busen, A. Ding, T. Schmitz-Rode, U. Steinseifer, J. Arens, G. Cattaneo, A novel plasma-based fluid for particle image velocimetry (PIV): In-Vitro feasibility study of flow diverter effects in Aneurysm model, Ann. Biomed. Eng. 46 (6) (2018) 841–848, http://dx.doi.org/10.1007/s10439-018-2002-1.

[69] A. Laurent, J.J. Durussel, J. Dufaux, L. Penhouët, A.L. Bailly, M. Bonneau, J.J. Merland, Effects of contrast media on blood rheology: Comparison in humans, pigs, and sheep, CardioVascular Interv. Radiol. 22 (1) (1999) 62–66, http://dx.doi.org/10.1007/s002709900330.

[70] B.J. Schürmann, P. Creutz, T. Schmitz-Rode, U. Steinseifer, J.C. Clauser, Ghost cells as a two-phase blood analog fluid: high-volume and high-concentration production, Artif. Organs. 49 (1) (2025) 31–38, http://dx.doi.org/10.1111/aor.14846, URL: https://onlinelibrary.wiley.com/doi/abs/10.1111/aor.14846 _eprint: https://onlinelibrary.wiley.com/doi/pdf/10.1111/aor.14846.

[71] D.E. Mann, J.M. Tarbell, Flow of non-Newtonian blood analog fluids in rigid curved and straight artery models, Biorheology 27 (5) (1990) 711–733, http://dx.doi.org/10.3233/bir-1990-27508.

[72] K.A. Brookshier, J.M. Tarbell, Evaluation of a transparent blood analog fluid: aqueous xanthan gum/glycerin, Biorheology 30 (2) (1993) 107–116, http://dx.doi.org/10.3233/bir-1993-30202.

[73] J. S. Horner, N. J. Wagner, A. N. Beris, A comparative study of blood rheology across species, Soft Matter 17 (18) (2021) 4766–4774, http://dx.doi.org/10.1039/D1SM00258A, URL: https://pubs.rsc.org/en/content/articlelanding/2021/sm/d1sm00258a, Publisher: Royal Society of Chemistry.

[74] C.P. Oates, Towards an ideal blood analogue for Doppler ultrasound phantoms, Phys. Med. Biol. 36 (11) (1991) 1433, http://dx.doi.org/10.1088/0031-9155/36/11/003.

[75] K.V. Ramnarine, D.K. Nassiri, P.R. Hoskins, J. Lubbers, Validation of a new Blood-Mimicking fluid for use in Doppler flow test objects, Ultrasound Med. Biol. 24 (3) (1998) 451–459, http://dx.doi.org/10.1016/S0301-5629(97)00277-9, URL: https://www.sciencedirect.com/science/article/pii/S0301562997002779.

[76] A. Thacker, S. Fu, R.L. Boni, L.H. Block, Inter- and Intra-Manufacturer variability in pharmaceutical grades and lots of Xanthan Gum, AAPS PharmSciTech 11 (4) (2010) 1619–1626, http://dx.doi.org/10.1208/s12249-010-9536-3.

[77] M.R.V.d. Moura, R.B.Z.L. Moreno, Concentration, brine salinity and temperature effects on Xanthan gum solutions rheology, Appl. Rheol. 29 (1) (2019) 69–79, http://dx.doi.org/10.1515/arh-2019-0007, URL: https://www.degruyter.com/document/doi/10.1515/arh-2019-0007/html.

[78] E.M. Nsengiyumva, M.P. Heitz, P. Alexandridis, Salt and temperature effects on Xanthan gum polysaccharide in aqueous solutions, Int. J. Mol. Sci. 25 (1) (2024) 490, http://dx.doi.org/10.3390/ijms25010490, URL: https://www.mdpi.com/1422-0067/25/1/490, Number: 1 Publisher: Multidisciplinary Digital Publishing Institute.

[79] E.M. Nsengiyumva, P. Alexandridis, Xanthan gum in aqueous solutions: Fundamentals and applications, Int. J. Biiol. Macromol. 216 (2022) 583–604, http://dx.doi.org/10.1016/j.ijbiomac.2022.06.189, URL: https://www.sciencedirect.com/science/article/pii/S0141813022014040.

[80] C.-E. Brunchi, M. Bercea, S. Morariu, M. Dascalu, Some properties of xanthan gum in aqueous solutions: effect of temperature and pH, J. Polym. Res. 23 (7) (2016) 123, http://dx.doi.org/10.1007/s10965-016-1015-4.

[81] J.A. Long, A. Ündar, K.B. Manning, S. Deutsch, Viscoelasticity of pediatric blood and its implications for the testing of a pulsatile pediatric blood pump, ASAIO J. 51 (5) (2005) 563, http://dx.doi.org/10.1097/01.mat.0000180353.12963.f2, URL: https://journals.lww.com/asaiojournal/abstract/2005/09000/viscoelasticity_of_pediatric_blood_and_its.24.aspx.

[82] N.A. Buchmann, M. Yamamoto, M. Jermy, T. David, Particle image velocimetry (PIV) and computational fluid dynamics (CFD) modelling of carotid Artery Haemodynamics under steady flow: A validation study, J. Biomech. Sci. Eng. 5 (4) (2010) 421–436, http://dx.doi.org/10.1299/jbse.5.421.

[83] P.H. Geoghegan, In Vitro Experimental Investigation Into the Effect of Compliance on Models of Arterial Hemodynamics (Ph.D. thesis), 2012.